Magnetic Resonance Imaging 63 (2019) 267–273

Contents lists available at ScienceDirect

Magnetic Resonance Imaging

journal homepage: www.elsevier.com/locate/mri

Original contribution

Evaluation of diffusion kurtosis imaging in stratification of nonalcoholic fatty liver disease and early diagnosis of nonalcoholic steatohepatitis in a rabbit model

Chang Li[a,b], Jing Ye[a], Yun Peng[a,b], Weiqiang Dou[c], Songan Shang[a,b], Jingtao Wu[a], Ramin Jafari[d], Kelly McCabe Gillen[d], Yi Wang[d,e], Martin Prince[d], Xianfu Luo[a,*]

[a] Department of Radiology, Northern Jiangsu People's Hospital, Clinical Medical School of Yangzhou University, No. 98 Nantong West Road, Yangzhou 225001, China
[b] Xiangya School of Medicine, Central South University, No. 172 Tongzipo Road, Changsha 410013, China
[c] GE Healthcare, MR Research China, Beijing, China
[d] Department of Radiology, Weill Medical College of Cornell University, 407 E 61st Street, New York, NY 10065, USA
[e] Department of Biomedical Engineering, Cornell University, Ithaca, NY, USA

ARTICLE INFO

Keywords:
Nonalcoholic fatty liver disease
Nonalcoholic steatohepatitis
Diffusion magnetic resonance imaging
Diagnostic imaging

ABSTRACT

Purpose: To examine the feasibility of MR diffusion kurtosis imaging (DKI) for characterizing nonalcoholic fatty liver disease (NAFLD) and diagnosing nonalcoholic steatohepatitis (NASH).

Methods: Thirty-two rabbits on high fat diet with different severities of NAFLD were imaged at 3 T MR including diffusion weighted imaging (DWI) and DKI using b values of 0, 400, 800 s/mm^2 with 15 diffusion directions at each b value. Apparent diffusion coefficient (ADC) was derived from the linear exponential DWI model. Mean diffusion (MD) and mean kurtosis (MK) were derived from the quadratic exponential model of DKI. Correlations between MR parameters and hepatic pathology determined by the NAFLD activity scoring system were analyzed by Spearman rank correlation analysis. Receiver operating characteristic analyses were applied to determine the cutoff values of MD, MK as well as ADC in distinguishing NASH from non-NASH. The diagnostic efficacies of MD and MK in detecting NASH were compared with that of ADC.

Results: Values for ADC and MD significantly decreased as the severity of NAFLD increased ($\rho = -0.529$, -0.904, respectively; $P < 0.05$). MK values significantly increased as the severity of NAFLD increased ($\rho = 0.761$; $P < 0.05$). In addition, both MD and MK values were significantly different between borderline NASH and NASH groups (MD: 1.729 ± 0.144 *vs.* $1.458 \pm 0.240[\times 10^{-3}\,\text{mm}^2/\text{s}]$; MK: 1.096 ± 0.079 *vs.* 1.237 ± 0.180; $P < 0.05$). Moreover, there was a significantly higher area under the curve (AUC) for both MD (0.955) and MK (0.905), as compared to ADC (0.736).

Conclusion: Diffusion kurtosis imaging was feasible for stratifying NAFLD, and more accurately discriminated NASH from non-NASH when compared with DWI.

1. Introduction

Nonalcoholic fatty liver disease (NAFLD) is the leading cause of chronic liver disease and has a rapidly increasing prevalence worldwide [1,2]. The pathological spectrum of NAFLD ranges from isolated or simple steatosis (SS) without inflammation, to the more aggressive nonalcoholic steatohepatitis (NASH) characterized by steatosis, lobular inflammation, and hepatocyte ballooning with varying degrees of fibrosis. Though NASH can progress to liver cirrhosis and even hepatocellular carcinoma, therapies to inhibit steatosis, inflammation, fibrosis and apoptosis are available to reverse NASH [3,4]. Accordingly, distinguishing NASH from simple steatosis is crucial for patient management.

Currently, percutaneous liver biopsy is the reference standard for diagnosing NASH [5]. Because of its invasiveness, potential complications and false negatives from sampling variability, biopsy is not widely accepted by clinicians or patients. Accurate, non-invasive imaging techniques are needed to diagnose NASH, monitor disease progression

Abbreviations: ADC, Apparent diffusion coefficient; DKI, Diffusion kurtosis imaging; FA, Fractional anisotropy; MD, Mean diffusion; MK, Mean kurtosis; NAFLD, Nonalcoholic fatty liver disease; NASH, Nonalcoholic steatohepatitis; SS, Simple steatosis

* Corresponding author.
E-mail address: xianfu-luo@hotmail.com (X. Luo).

https://doi.org/10.1016/j.mri.2019.08.032
Received 6 June 2019; Received in revised form 19 August 2019; Accepted 21 August 2019

and evaluate treatment response [6]. Laboratory tests such as cytokeratin-18 (CK-18) and serum aminotransferase, and several NAFLD diagnostic panels (Fatty Liver Index, SteatoTest, NAFLD liver Fat Score and Lipid accumulation product) still lack specificity for diagnosing NASH [7].

Noninvasive magnetic resonance (MR) techniques, such as proton MR spectroscopy (H^1-MRS) and water-fat separation MR imaging (IDEAL-IQ or Dixon) with proton density fat fraction (PDFF), have been used to measure hepatic fat [8,9]. However, these methods are not able to provide information regarding hepatic inflammation and fibrosis. MR diffusion weighted imaging (DWI) to measure molecule motion has been used in NAFLD. The apparent diffusion coefficient (ADC) from a mono-exponential model [10] or diffusivity (D) and perfusion fraction (f) from a bi-exponential model, suggest that ADC and D are well correlated with hepatic fat fraction but not with hepatic inflammation [11,12]. Diffusion kurtosis imaging (DKI), is a more advanced DWI method that is sensitive to non-Gaussian distribution of molecular motion [13], which has been useful for diagnosing liver fibrosis and malignant hepatic lesions [14,15]. DKI has yet to be applied to NAFLD.

We hypothesize that DKI is sensitive to hepatic steatosis, inflammation, hepatocyte ballooning, and fibrosis for assessing NAFLD severity and distinguishing between NASH and simple steatosis. We report here DKI as well as conventional DWI on a preclinical rabbit model encompassing both simple steatosis and NASH induced by high fat/cholesterol diet.

2. Materials and methods

2.1. Animal model

This study was approved by the animal care and use committee. Thirty-two male New Zealand rabbits weighing approximately 2.5 kg were randomly divided into a normal diet group ($n = 6$) and a high fat diet group ($n = 26$). All rabbits were kept in independent cages at room temperature (21 ± 2 °C). The diurnal circle was 12 h. The weight of chow was restricted to 100 g per-rabbit per-day. Rabbits in the normal diet group ($n = 6$), were fed a standard diet (Product No. TP2R001, Trophic Animal Feed high-tech Co. Ltd., China) for 3 weeks. To induce different NAFLD, twenty-six rabbits were fed a high fat/cholesterol diet (standard diet supplemented with 2% cholesterol and 10% triglycerides, Product No. TP2R144; Trophic Animal Feed high-tech Co.Ltd., China) for 1 week ($n = 6$), 3 weeks ($n = 6$), 4 weeks ($n = 6$), and 8 weeks ($n = 8$) to achieve different degrees of NAFLD severity ranging from simple steatosis (1 week) to high grade NASH (8 weeks) [16].

2.2. Magnetic resonance imaging

All MRI experiments were performed on a clinical 3.0 T MR imaging system (Discovery 750 W, GE, USA) with a 16-channel surface coil (GEM Flex). Each rabbit was anesthetized with auricular injection of pentobarbital sodium, laterally positioned, and fixed with adhesive tape to reduce movement artifact. Free-breathing liver DKI and DWI were performed using axial single shot echo planar imaging, as previously reported [17,18] using the following parameters: TR/TE = 2500/77.4 msec. Three b values (0, 400 and 800 s/mm^2) with 15 diffusion directions at each b value were acquired and attained sufficient signal to noise ratio (SNR). The remaining parameters were: matrix 128 × 128 pixels; slice number 9; slice thickness 3.0 mm; slice space 0.3 mm; field of view (FOV) 15.0 mm × 10.0 mm. The acquisition time was 2 min 38 s. The pentobarbital sodium reduced the respiratory rate and tidal volumes sufficiently to minimize respiratory motion artifacts.

For DWI, the sequence parameters were: repetition time/echo time 2500/77.4 msec; matrix size 128 × 128 pixels; slice number 9; slice thickness 3.0 mm; FOV 15.0 mm × 10.0 mm. The choice of b values was 0 and 600 s/mm^2. The acquisition time was 1 min 25 s.

2.3. Imaging analysis

Two radiologists with 5 and 12 years of experience in abdominal imaging, were blinded to the diet and the histological grade of each rabbit, and analyzed all images on a computer workstation (Advantage Workstation 4.6 GE, USA). DKI-derived parameters, including fractional anisotropy (FA), mean diffusion (MD, D) and mean kurtosis (MK, K) as [15]: $S(b) = S(0)\exp(-b{\cdot}D + b^2{\cdot}D^2{\cdot}K/6)$, where b represents each applied b-value and S(0) is the signal intensity at b = 0 s/mm^2. For comparison, ADC values based on DWI images were calculated by using a monoexponential model [19]: $S(b) = S(0)\exp(-b{\cdot}ADC)$. For each rabbit, three circular regions of interest (ROI) with areas ranging from 30 to 50 mm^2 were delineated within liver parenchyma on ADC and DKI parametric maps (FA, MD, MK). ROI placement was chosen to exclude large hepatic vessels and artifacts. The 3 ROIs were placed on different slices and in three different liver regions being careful to stay away from the stomach which commonly had susceptibility artifact from gastric air. These ROIs were automatically propagated between each parametric map. The six ROI measurements (3 from each radiologist) were averaged for further statistical analysis.

2.4. Histopathological analysis

All rabbits were sacrificed directly after the MRI experiments. Liver samples were immersed in 10% phosphate-buffered formalin, paraffin embedded, and sectioned. Hematoxylin and eosin, and Masson's trichrome staining were performed on each sample. The slides were reviewed by a pathologist with 15 years of experience in liver pathology, who was blinded to the rabbit diets and imaging data. The NASH clinical research network's (NASH CRN) NAFLD Activity Score (NAS) was used to develop a score for each rabbit [20], which was the sum of semi-quantitatively determined indicators including steatosis (0–3 points), acinar inflammation (0–3 points) and hepatocellular ballooning (0–2 points). It thus determined normal (NAS = 0), simple steatosis (SS) (NAS = 1, 2), borderline NASH (NAS = 3, 4) and NASH (NAS ≥ 5). METAVIR scoring system was used to evaluate the degree of fibrosis [21], in which F0 = no relevant fibrosis, F1 = zone 3 perisinusoidal fibrosis or portal, F2 = zone 3 perisinusoidal fibrosis and periportal fibrosis, F3 = bridging fibrosis and F4 = cirrhosis.

2.5. Statistical analysis

All statistical analyses were performed with SPSS software (version 20.0, SPSS; Chicago) and MedCalc (version 17.6, Mariakerke, Belgium). The Shapiro-Wilk test was used to determine the normality of diffusion parameters (ADC, FA, MD and MK). Gaussian distribution variables were expressed as mean with standard deviation (SD). Intra-class correlation (ICC) coefficient analysis was used to assess the inter-observer reproducibility of MRI measurements. Diffusion parameters (ADC, FA, MD and MK) between the different NAFLD groups were compared by one-way analysis of variance and least significant difference test. Spearman rank correlation analysis was performed to compare the correlations between ADC, FA, MD, MK and the severity of NAFLD. To identify which pathological features (steatosis, acinar inflammation, hepatocellular ballooning and fibrosis), caused the greatest impact on DWI and DKI derived parameters (ADC, MD, MK), multivariate stepwise regression analysis was performed. Variables with $P > 0.1$ at univariate analysis were removed in the regression model. Additionally, receiver operating characteristic curve (ROC) analysis was performed to assess the diagnostic performance of ADC, MD and MK for NAFLD grading. The optimal cutoff values were defined as the value that maximized the sum of the sensitivity and specificity; the corresponding sensitivities and specificities were also obtained. ROC curves were compared to evaluate the diagnostic efficacies of ADC, MD and MK in predicting NASH. $P < 0.05$ was considered statistically significant.

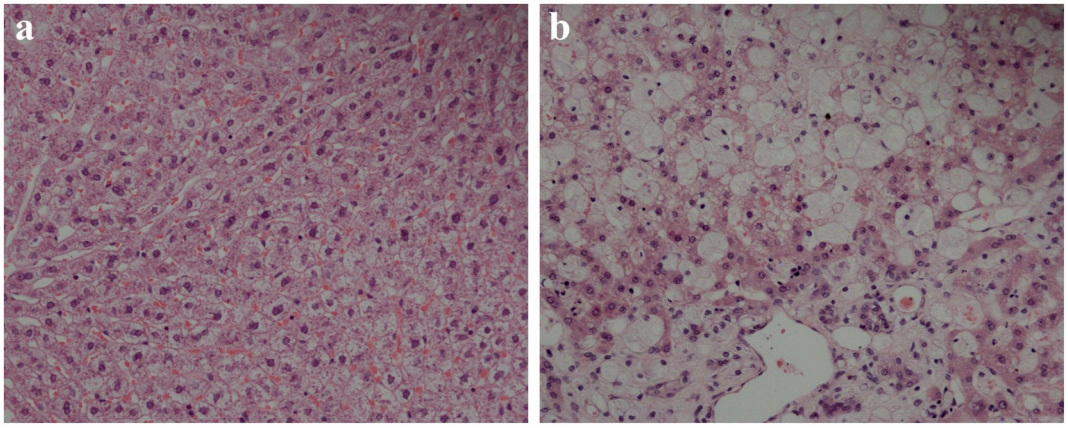

Fig. 1. Photomicrograph of normal liver specimen (a). Photomicrograph of NASH liver specimen (b). Fat accumulation and ballooning degeneration in hepatic cells with lobular inflammation were showed in the NASH (hematoxylin-eosin stain; magnification, ×200).

3. Results

3.1. Histopathology

Liver specimens from high fat/cholesterol diets showed a homogeneous increase in microvesicular steatosis and ballooning degeneration of hepatocytes with scattered lobular inflammation; these pathological changes corresponded to the duration of the high fat diet. (Fig. 1).

In the normal diet group, all 6 rabbits had normal livers with NAS = 0. In comparison, after one week on the high fat/cholesterol diet, 5 out of 6 rabbit livers were classified as simple steatosis and the other was normal. After 3 weeks on the high fat/cholesterol diet, 3 rabbit livers were classified as simple steatosis and the remaining 3 were borderline NASH. After 4 weeks on the high fat/cholesterol diet, 3 livers were classified as borderline NASH and other 3 were NASH. After 8 weeks on the high fat/cholesterol diet, all 8 rabbit livers were classified as NASH. In total, there were 7 rabbits with normal liver, 8 with simple steatosis, 6 with borderline NASH, and 11 with NASH.

According to the METAVIR scoring system, all 7 rabbits with normal liver and 8 with simple steatosis scored F0. In addition, 3 of 6 animals whose livers were classified as borderline NASH were scored F0; the remaining 3 were scored F1. One of the 11 livers in the NASH group was scored F2 and the remaining ten were scored F1. No F3 and F4 liver specimens were detected in our study.

3.2. MR measurements in NAFLD groups with different severities

Inter-observer agreement was high with intra-class correlation coefficients (ICC) values of 0.897, 0.885, 0.969, 0.927, for ADC, FA, MD, and MK, respectively. Mean levels of ADC, FA, MD and MK values for the normal, simple steatosis, borderline NASH and NASH groups were in Table 1. MD was the only parameter in which the values were statistically different between all groups: normal *vs.* simple steatosis (2.434 ± 0.251 *vs.* 1.973 ± 0.185 [$\times 10^{-3}$ mm^2/s]), simple steatosis *vs.* borderline NASH (1.973 ± 0.185 *vs.* 1.729 ± 0.114 [$\times 10^{-3}$ mm^2/s]), and borderline *vs.* NASH (1.729 ± 0.114 *vs.* 1.458 ± 0.240 [$\times 10^{-3}$ mm^2/s]). In addition, MK showed significantly different values between the borderline and NASH groups (1.096 ± 0.079 *vs.* 1.237 ± 0.180), but no significant difference was found between normal and simple steatosis, nor between simple steatosis and borderline NASH (Fig. 2).

3.3. Correlation between diffusion parameters and NAFLD severity

As NAFLD severity increased, both MD and ADC were negatively correlated, with correlation coefficients of −0.905 and − 0.529, respectively ($P < 0.05$). In contrast, a positive correlation was found between NAFLD progression and MK ($\rho = 0.761$; $P < 0.05$). For FA values, no significant correlation with NAFLD severity was observed ($\rho = 0.030$; $P = 0.869$) (Table 1). Examples of ADC, FA, MD and MK pseudo-color maps from the normal liver and NASH groups are shown in Fig. 3.

Stepwise multiple regression analysis including the four histological variables (steatosis, acinar inflammation, hepatocellular ballooning, and fibrosis) showed MD significantly correlated only with hepatocellular steatosis (R^2-adjusted = 0.711; $P < 0.001$). In contrast, ADC and MK significantly correlated with hepatocellular ballooning (ADC: R^2-adjusted = 0.275; MK: R^2-adjusted = 0.496; $P < 0.001$).

3.4. Receiver operating characteristics curve analysis

ROC curve analysis including area under the ROC curve (AUC), cutoff values, sensitivities and specificities for differentiating NASH from non-NASH livers were listed in Table 2.

Comparing ROC curves analysis, MD (AUC = 0.955) and MK (AUC = 0.905) showed significantly greater AUC values than ADC (AUC = 0.727), indicating more robust performance in differentiating

Table 1
Association of Diffusion Parameters (ADC, FA, MD, MK) with NAFLD Severity Groups.

Parameters	Normal histology ($n = 7$)	Simple steatosis ($n = 8$)	Borderline NASH ($n = 6$)	NASH ($n = 11$)	ρ	P
ADC ($\times 10^{-3}$ mm^2/s)	1.338 ± 0.222	1.225 ± 0.264	1.063 ± 0.149	1.041 ± 0.168	−0.529	0.002
FA (%)	0.609 ± 0.031	0.637 ± 0.033	0.614 ± 0.048	0.618 ± 0.042	0.030	0.869
MD ($\times 10^{-3}$ mm^2/s)	2.434 ± 0.251	1.973 ± 0.185	1.729 ± 0.114	1.458 ± 0.240	−0.905	< 0.001
MK	0.964 ± 0.090	1.047 ± 0.058	1.096 ± 0.079	1.237 ± 0.180	0.761	< 0.001

Data expressed as means ± standard deviation. Spearman rank correlation analysis was performed to compare the correlations between ADC, FA, MD, MK and the severity of NAFLD. ρ, Spearman correlation coefficient. ADC, apparent diffusion coefficient; FA, fractional anisotropy; MD, mean diffusion; MK, mean kurtosis.

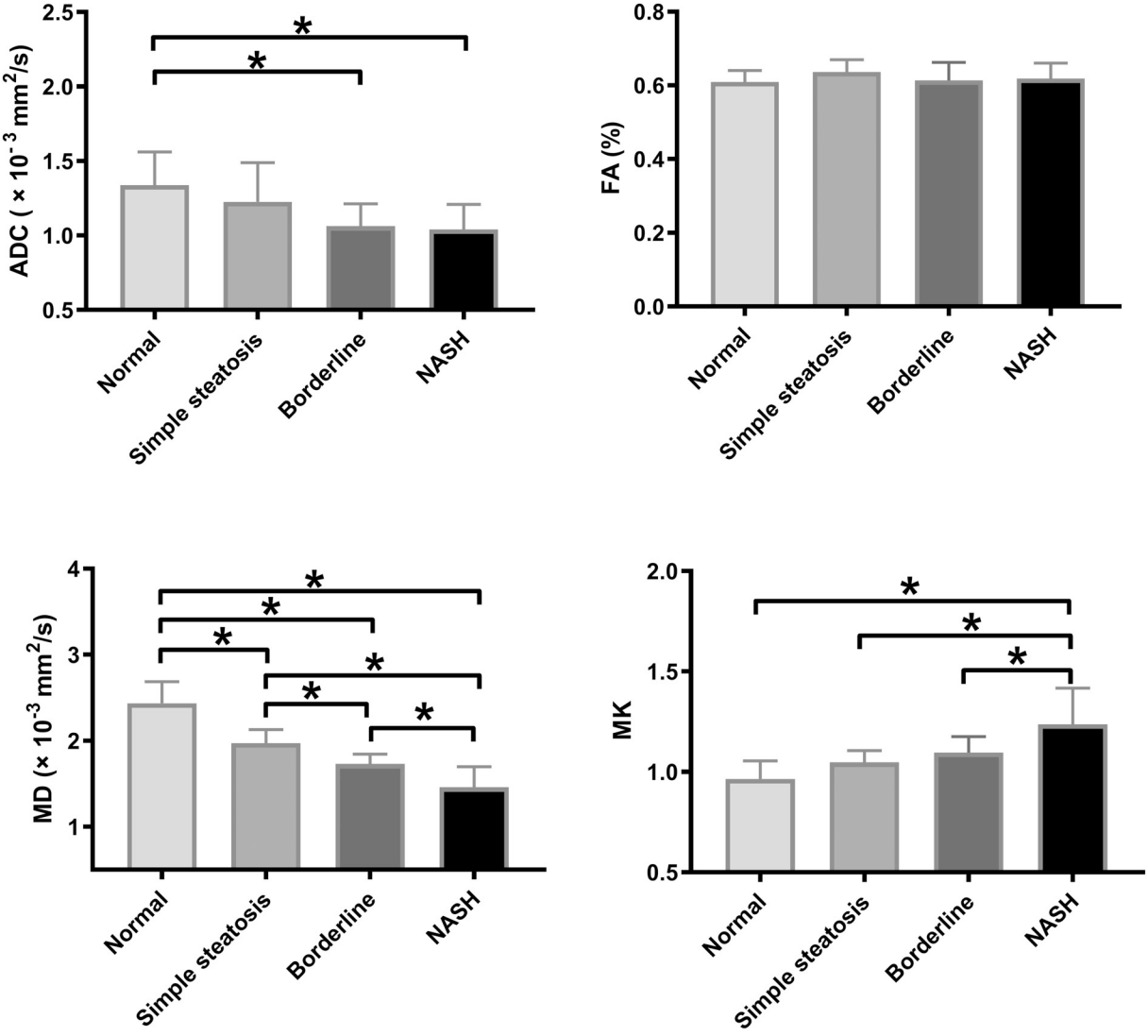

Fig. 2. Histograms of diffusion parameter values at different severities of NAFLD groups based on NAS scoring system. MD was the only parameter showing significant differences between each NAFLD groups. Both MD and MK showed significant difference between the borderline and NASH groups (*$P < 0.05$).

NASH from non-NASH ($P < 0.05$). No significant difference was found between MD and MK in differentiating NASH from non-NASH (Fig. 4).

4. Discussion

These data from 32 rabbits with diet induced fatty liver demonstrate that NAFLD severity can be evaluated by diffusion kurtosis imaging (DKI). MK and MD significantly correlated with NAFLD severity. Both MK and MD values were significantly different between the borderline NASH and NASH groups. Furthermore, the diagnostic accuracies of MD and MK from the DKI model were higher than that of ADC in the differentiation of NASH from non-NASH. Compared with mono-exponential DWI, DKI appears to reveal non-Gaussian water diffusion information in the tissue microenvironment affected by NAFLD pathology. MK and MD are promising diffusion biomarkers for early detection of NASH.

MD reflects mean values of molecular diffusion in multiple directions obtained from the DKI model. Previous studies indicated that MD yielded a more accurate diffusion metric than ADC [17,22]. Similarly, our study also showed that MD ($\rho = -0.905$) had a larger correlation coefficient with NAFLD severity than ADC ($\rho = -0.529$). In addition, when compared to ADC, MD had a higher diagnostic accuracy (greater AUC) in distinguishing NASH from non-NASH ($P < 0.05$). As NAFLD progresses, increasing intracellular triglycerides cause hepatocellular ballooning, narrowed sinusoids, and extracellular inflammation restricting water molecular diffusion both intracellularly and extracellularly [23,24]. These new populations of restricted water protons skew the normal distribution of diffusivity creating a non-Gaussian distribution that is detected with DKI but not correctly modeled with mono-exponential ADC [25,26].

Another parameter in this non-Gaussian diffusion model, MK, accounts for additional complexity of the microenvironment and its magnitude of deviation from Gaussian diffusion in biological tissues [27]. Anderson *et al.* [28] and Hu *et al.* [29] reported that MK reflected liver microstructural complexity and positively correlated with fibrosis stage. The current study showed that MK increased with increasing NAFLD severity and was independently associated with hepatocellular ballooning but not with steatosis, acinar inflammation, or fibrosis. Of note, Li *et al.* [30] reported that of these variables, fibrosis was the only variable associated with MK in liver fibrosis, but our results indicated that there was no independent association between fibrosis and MK. This discordance may be because our study only included one rabbit with F2. Lack of fibrosis in our rabbit model reflected the short duration of NASH which takes longer to develop cirrhosis. However, our goal was to detect the early findings of NASH before liver fibrosis becomes irreversible; so, the model was useful in this regard. Although fibrosis

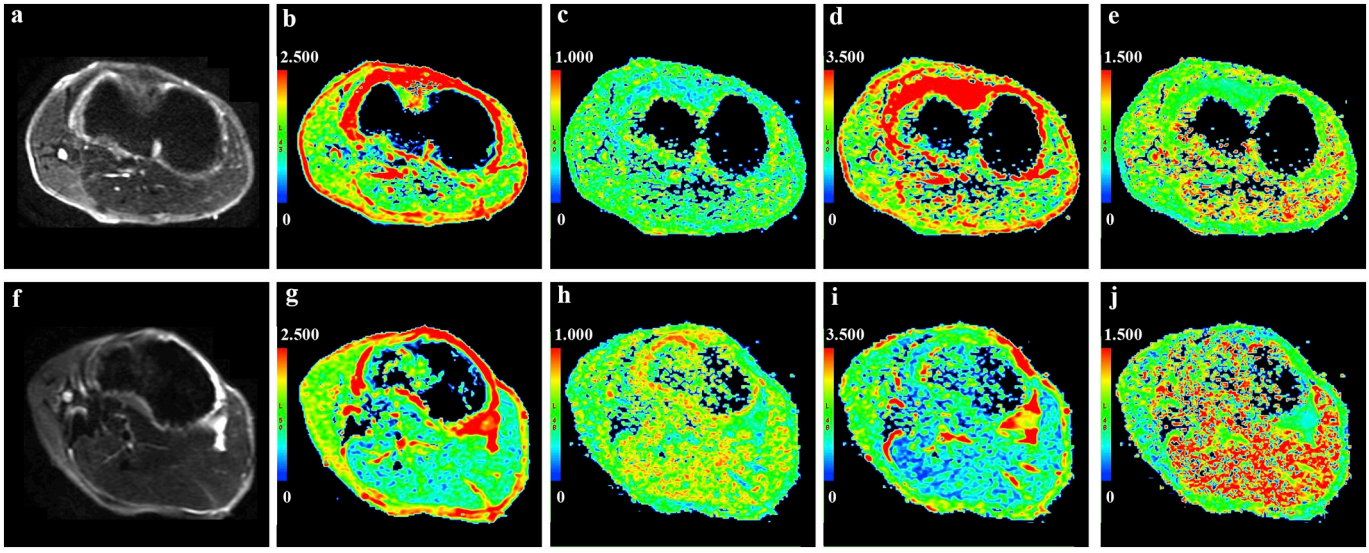

Fig. 3. Diffusion parameters maps of normal liver (upper images a–e, on standard diet feeding) and nonalcoholic steatohepatitis (lower images f-j, on high fat/cholesterol diet feeding for 8 weeks). a is a representative DWI image at b value of 0 s/mm^2 and b-e are pseudo-color maps of ADC, FA, MD, and MK with mean values of 1.360×10^{-3} mm^2/s, 60.4%, 2.313×10^{-3} mm^2/s and 0.999, respectively. f is an exemplary DWI image at b value of 0 s/mm^2 and g-j are pseudo-color maps of ADC, FA, MD and MK with mean values of 0.847×10^{-3} mm^2/s, 69.2%, 1.197×10^{-3} mm^2/s and 1.392, respectively.

was not prominent in our study, the presence of steatosis, inflammation, necrosis, hepatocellular ballooning and hepatocyte regeneration was changing the microscopic structure causing larger MK.

Conventional DWI assumes that water molecules are moving randomly and therefore can provide information about the extracellular space. Previous studies showed that ADC and fat fraction had an inverse relationship, likely because diffusion of water molecules was restricted by fat accumulation [10,31]. Joo [11] reported that the ADC value was decreased in a NAFLD group as compared to the normal group, but it did not correlate with NAFLD severity ($\rho = -0.27$; $P = 0.17$). Our data show ADC was inversely correlated with NAFLD severity ($\rho = -0.529$; $P = 0.002$), but unable to differentiate borderline NASH from NASH. Joo *et al.* [11] staged NAFLD in rabbits using multi-b values in DWI (intravenous incoherent motion, IVIM), in which diffusion and perfusion could be separately obtained. In their study, the perfusion fraction (f) decreased with increasing severity of NAFLD and was able to distinguish NASH from non-NASH. However, Guiu *et al.* [12] demonstrated that f increased in steatotic compared with nonsteatotic patients. Thus, the accuracy of the IVIM model in stratifying NAFLD needs to be further validated. MR imaging with specialized contrast agents such as bis-hydroxy-tryptamide-diethylenetriaminepentaacetate gadolinium (MPO-Gd), ultrasmall superparamagnetic iron oxide particle (USPIO) or gadolinium ethoxybenzyl diethylenetriamine pentaacetic acid (Gd-EOB-DTPA) might assess the inflammatory activity in NAFLD [32–35]. However, these add cost/complexity to the MRI exam and possible allergic reactions and renal injury may contraindicate contrast administration in some patients.

Limitations of this study include a relatively small number of rabbits ($n = 32$), however the observations are statistically significant. Second, the NAFLD rabbit models induced by high fat/cholesterol diet feeding may be different from human NAFLD. In particular humans often have more fibrosis. A rabbit model with more fibrosis may be possible by extending the high fat/cholesterol diet beyond 8 weeks. Third, all liver MR imaging was performed during free breathing with limits image quality and may result in imperfect registration of images with different b values in patients. Respiratory motion was minimized in these rabbits with sodium pentobarbital anesthesia to reduce respiratory rate and tidal volumes. Fourth, the maximum b value of our study was 800 s/mm^2, higher b values can be used to quantify non-Gaussian diffusions parameters more precisely but our preliminary scanning showed that

Table 2
Receiver operating characteristics curve analysis of MR parameters for stratifying NAFLD.

NAFLD Stages	Parameters	AUC	95%CI(AUC)	Cutoff values	Sensitivity (%)	Specificity (%)
Normal (n = 7)	ADC($\times 10^{-3}$mm^2/s)	0.811	0.634 - 0.927	1.240	80.00	85.71
vs.	MD($\times 10^{-3}$mm^2/s)	0.989	0.870 - 1.000	2.040	96.00	100.00
≥ Simple steatosis (n = 25)	MK	0.894	0.734 - 0.975	0.943	100.00	71.43
≤ Simple steatosis (n = 15)	ADC($\times 10^{-3}$mm^2/s)	0.800	0.621- 0.900	1.240	94.12	66.67
vs.	MD($\times 10^{-3}$mm^2/s)	0.973	0.844 - 1.000	1.800	94.12	93.33
≥ Borderline (n = 17)	MK	0.884	0.722 - 0.970	1.153	64.71	100.00
≤ Borderline (n = 21)	ADC($\times 10^{-3}$mm^2/s)	0.727	0.542 - 0.896	1.200	90.91	57.14
vs.	MD($\times 10^{-3}$mm^2/s)	0.955	0.816 - 0.997	1.600	81.82	95.24
NASH (n = 11)	MK	0.905	0.748 - 0.980	1.157	81.82	95.24

The diagnostic performance of ADC, MD and MK for NAFLD grading were assessed by receiver operating characteristic curve analysis. The optimal cutoff values were defined as the value that maximized the sum of the sensitivity and specificity; the corresponding sensitivities and specificities were also obtained. ADC, apparent diffusion coefficient; MD, mean diffusion; MK, mean kurtosis.

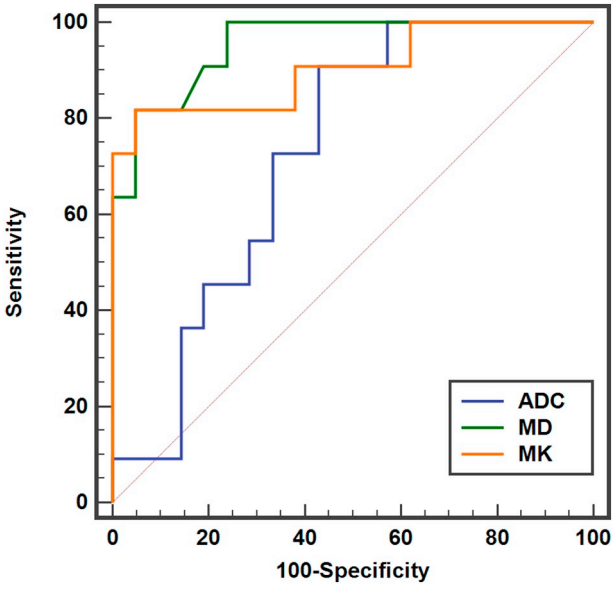

Fig. 4. Diagnostic ability of ADC, MD and MK for discriminating NASH from non-NASH groups. Both MD and MK showed higher AUC values than ADC ($P < 0.05$).

higher b values had too much noise for accurate post processing [18]. A larger sample of human NAFLD patients scanned with higher b-values might provide more reliable values of DKI in stratifying NAFLD.

In conclusion, this study demonstrated that DKI was feasible for noninvasive stratification of NAFLD in a rabbit model. Both DKI-derived metrics, MD and MK, showed more robust performance compared to conventional diffusion parameter ADC in differentiating NASH from non-NASH. Therefore, DKI could serve as a robust technique to stratify NAFLD, and might have potential to be used in early diagnosis of nonalcoholic steatohepatitis. DKI will be tested in patients with NAFLD for further validation.

Declaration of competing interest

We declare that we have no conflicts of interest.

Acknowledgements

None.

Funding

This study was funded by the Natural Science Foundation of Youth Fund project from Science and Technology Department of Jiangsu Province (BK20160450); Top Six Talent Summit Project of Jiangsu Province Human Resources and Social Security Department (2016-WSN-277); Jiangsu Provincial Government Scholarship for Studying Abroad (JS-2018-229) Jiangsu Provincial Youth Talents Program for Medicine (QNRC2016321); Yangzhou Municipal Youth Talents Program for Medicine (YZZDRC201816); Science and Technology project of Yangzhou (YZ2018059).

References

[1] Benedict M, Zhang X. Non-alcoholic fatty liver disease: an expanded review. World J Hepatol 2017;9(16):715–32. https://doi.org/10.4254/wjh.v9.i16.715.
[2] Calzadilla Bertot L, Adams LA. The natural course of non-alcoholic fatty liver disease. Int J Mol Sci 2016;17(5). https://doi.org/10.3390/ijms17050774.
[3] Sayiner M, Koenig A, Henry L, Younossi ZM. Epidemiology of nonalcoholic fatty liver disease and nonalcoholic steatohepatitis in the United States and the rest of the world. Clin Liver Dis 2016;20(2):205–14. https://doi.org/10.1016/j.cld.2015.10.001.
[4] Kanwar P, Kowdley KV. The metabolic syndrome and its influence on nonalcoholic steatohepatitis. Clin Liver Dis 2016;20(2):225–43. https://doi.org/10.1016/j.cld.2015.10.002.
[5] Nalbantoglu IL, Brunt EM. Role of liver biopsy in nonalcoholic fatty liver disease. World J Gastroenterol 2014;20(27):9026–37. https://doi.org/10.3748/wjg.v20.i27.9026.
[6] Regev A, Berho M, Jeffers LJ, Milikowski C, Molina EG, Pyrsopoulos NT, et al. Sampling error and intraobserver variation in liver biopsy in patients with chronic HCV infection. Am J Gastroenterol 2002;97(10):2614–8. https://doi.org/10.1111/j.1572-0241.2002.06038.x.
[7] Tsai E, Lee TP. Diagnosis and evaluation of nonalcoholic fatty liver disease/non-alcoholic steatohepatitis, including noninvasive biomarkers and transient elastography. Clin Liver Dis 2018;22(1):73–92. https://doi.org/10.1016/j.cld.2017.08.004.
[8] Dulai PS, Sirlin CB, Loomba R. MRI and MRE for non-invasive quantitative assessment of hepatic steatosis and fibrosis in NAFLD and NASH: clinical trials to clinical practice. J Hepatol 2016;65(5):1006–16. https://doi.org/10.1016/j.jhep.2016.06.005.
[9] Tang A, Tan J, Sun M, Hamilton G, Bydder M, Wolfson T, et al. Nonalcoholic fatty liver disease: MR imaging of liver proton density fat fraction to assess hepatic steatosis. Radiology 2013;267(2):422–31. https://doi.org/10.1148/radiol.12120896.
[10] Poyraz AK, Onur MR, Kocakoc E, Ogur E. Diffusion-weighted MRI of fatty liver. Journal of magnetic resonance imaging: JMRI 2012;35(5):1108–11. https://doi.org/10.1002/jmri.23519.
[11] Joo I, Lee JM, Yoon JH, Jang JJ, Han JK, Choi BI. Nonalcoholic fatty liver disease: intravoxel incoherent motion diffusion-weighted MR imaging-an experimental study in a rabbit model. Radiology 2014;270(1):131–40. https://doi.org/10.1148/radiol.13122506.
[12] Guiu B, Petit JM, Capitan V, Aho S, Masson D, Lefevre PH, et al. Intravoxel incoherent motion diffusion-weighted imaging in nonalcoholic fatty liver disease: a 3.0-T MR study. Radiology 2012;265(1):96–103. https://doi.org/10.1148/radiol.12112478.
[13] Jensen JH, Helpern JA, Ramani A, Lu H, Kaczynski K. Diffusional kurtosis imaging: the quantification of non-Gaussian water diffusion by means of magnetic resonance imaging. Magn Reson Med 2005;53(6):1432–40. https://doi.org/10.1002/mrm.20508.
[14] Budjan J, Sauter EA, Zoellner FG, Lemke A, Wambsganss J, Schoenberg SO, et al. Diffusion kurtosis imaging of the liver at 3 Tesla: in vivo comparison to standard diffusion-weighted imaging. Acta Radiol 2018;59(1):18–25. https://doi.org/10.1177/0284185117706608.
[15] Wang WT, Yang L, Yang ZX, Hu XX, Ding Y, Yan X, et al. Assessment of microvascular invasion of hepatocellular carcinoma with diffusion kurtosis imaging. Radiology 2018;286(2):571–80. https://doi.org/10.1148/radiol.2017170515.
[16] Kainuma M, Fujimoto M, Sekiya N, Tsuneyama K, Cheng C, Takano Y, et al. Cholesterol-fed rabbit as a unique model of nonalcoholic, nonobese, non-insulin-resistant fatty liver disease with characteristic fibrosis. J Gastroenterol 2006;41(10):971–80. https://doi.org/10.1007/s00535-006-1883-1.
[17] Yoshimaru D, Miyati T, Suzuki Y, Hamada Y, Mogi N, Funaki A, et al. Diffusion kurtosis imaging with the breath-hold technique for staging hepatic fibrosis: a preliminary study. Magn Reson Imaging 2018;47:33–8. https://doi.org/10.1016/j.mri.2017.11.001.
[18] Filli L, Wurnig M, Nanz D, Luechinger R, Kenkel D, Boss A. Whole-body diffusion kurtosis imaging: initial experience on non-Gaussian diffusion in various organs. Invest Radiol 2014;49(12):773–8. https://doi.org/10.1097/RLI.0000000000000082.
[19] Le Bihan D, Breton E, Lallemand D, Aubin ML, Vignaud J, Laval-Jeantet M. Separation of diffusion and perfusion in intravoxel incoherent motion MR imaging. Radiology 1988;168(2):497–505. https://doi.org/10.1148/radiology.168.2.3393671.
[20] Hjelkrem M, Stauch C, Shaw J, Harrison SA. Validation of the non-alcoholic fatty liver disease activity score. Aliment Pharmacol Ther 2011;34(2):214–8. https://doi.org/10.1111/j.1365-2036.2011.04695.x.
[21] Poynard T, Bedossa P, Opolon P. The OBSVIRC, METAVIR, CLINIVIR, and DOSVIRC groups. Natural history of liver fibrosis progression in patients with chronic hepatitis C. Lancet 1997;349(9055):825–32. https://doi.org/10.1016/S0140-6736(96)07642-8.
[22] Shi RY, Yao QY, Zhou QY, Lu Q, Suo ST, Chen J, et al. Preliminary study of diffusion kurtosis imaging in thyroid nodules and its histopathologic correlation. Eur Radiol 2017;27(11):4710–20. https://doi.org/10.1007/s00330-017-4874-0.
[23] Ijaz S, Yang W, Winslet MC, Seifalian AM. Impairment of hepatic microcirculation in fatty liver. Microcirculation 2003;10(6):447–56. https://doi.org/10.1038/sj.mn.7800206.
[24] McCuskey RS, Ito Y, Robertson GR, McCuskey MK, Perry M, Farrell GC. Hepatic microvascular dysfunction during evolution of dietary steatohepatitis in mice. Hepatology 2004;40(2):386–93. https://doi.org/10.1002/hep.20302.
[25] Rosenkrantz AB, Padhani AR, Chenevert TL, Koh DM, De Keyzer F, Taouli B, et al. Body diffusion kurtosis imaging: basic principles, applications, and considerations for clinical practice. J Magn Reson Imaging 2015;42(5):1190–202. https://doi.org/10.1002/jmri.24985.
[26] Sheng RF, Wang HQ, Yang L, Jin KP, Xie YH, Chen CZ, et al. Diffusion kurtosis imaging and diffusion-weighted imaging in assessment of liver fibrosis stage and necroinflammatory activity. Abdominal radiology 2017;42(4):1176–82. https://doi.org/10.1007/s00261-016-0984-4.
[27] Bai Y, Lin Y, Tian J, Shi D, Cheng J, Haacke EM, et al. Grading of gliomas by using monoexponential, biexponential, and stretched exponential diffusion-weighted MR

imaging and diffusion kurtosis MR imaging. Radiology 2016;278(2):496–504. https://doi.org/10.1148/radiol.2015142173.
[28] Anderson SW, Barry B, Soto J, Ozonoff A, O'Brien M, Jara H. Characterizing non-Gaussian, high b-value diffusion in liver fibrosis: stretched exponential and diffusional kurtosis modeling. Journal of magnetic resonance imaging : JMRI 2014;39(4):827–34. https://doi.org/10.1002/jmri.24234.
[29] Hu G, Liang W, Wu M, Chan Q, Li Y, Xu J, et al. Staging of rat liver fibrosis using monoexponential, stretched exponential and diffusion kurtosis models with diffusion weighted imaging- magnetic resonance. Oncotarget 2018;9(2):2357–66. https://doi.org/10.18632/oncotarget.23413.
[30] Yang L, Rao S, Wang W, Chen C, Ding Y, Yang C, et al. Staging liver fibrosis with DWI: is there an added value for diffusion kurtosis imaging? Eur Radiol 2018;28(7):3041–9. https://doi.org/10.1007/s00330-017-5245-6.
[31] Anderson SW, Soto JA, Milch HN, Ozonoff A, O'Brien M, Hamilton JA, et al. Effect of disease progression on liver apparent diffusion coefficient values in a murine model of NASH at 11.7 Tesla MRI. Journal of magnetic resonance imaging : JMRI 2011;33(4):882–8. https://doi.org/10.1002/jmri.22481.
[32] Pulli B, Wojtkiewicz G, Iwamoto Y, Ali M, Zeller MW, Bure L, et al. Molecular MR imaging of myeloperoxidase distinguishes steatosis from steatohepatitis in non-alcoholic fatty liver disease. Radiology 2017;284(2):390–400. https://doi.org/10.1148/radiol.2017160588.
[33] Smits LP, Coolen BF, Panno MD, Runge JH, Nijhof WH, Verheij J, et al. Noninvasive differentiation between hepatic steatosis and steatohepatitis with MR imaging enhanced with USPIOs in patients with nonalcoholic fatty liver disease: a proof-of-concept study. Radiology 2016;278(3):782–91. https://doi.org/10.1148/radiol.2015150952.
[34] Yamada T, Obata A, Kashiwagi Y, Rokugawa T, Matsushima S, Hamada T, et al. Gd-EOB-DTPA-enhanced-MR imaging in the inflammation stage of nonalcoholic steatohepatitis (NASH) in mice. Magn Reson Imaging 2016;34(6):724–9. https://doi.org/10.1016/j.mri.2016.03.009.
[35] Xie Y, Zhang H, Jin C, Wang X, Wang X, Chen J, et al. Gd-EOB-DTPA-enhanced T1rho imaging vs diffusion metrics for assessment liver inflammation and early stage fibrosis of nonalcoholic steatohepatitis in rabbits. Magn Reson Imaging 2018;48:34–41. https://doi.org/10.1016/j.mri.2017.12.017.